CERN-LCGAPP-2007-01
March 2, 2007
Version 1.0

Third Benchmark Study for Validation of Hadronic Physics Simulations at LHC: Inclusive Charged Pion Production in Hadron-Nucleus Interactions at 100 and 320 GeV/c

A. Ribon
CERN PH-SFT

Abstract

In this note we present the validation of Fluka and Geant4 simulation packages on a thin-target benchmark, consisting of 100 GeV/c beams of π^+, π^-, K^+, p, and $\overline{p}$, and 320 GeV/c beam of π^- on foils of Mg, Ag, and Au. The distributions considered are the laboratory rapidity, and the transverse momentum squared of positive and negative pions produced by the collisions.

1 Experimental apparatus

Details of the experimental apparatus, the analysis, and results which we use in this benchmark are described in [1]. We recall briefly here only the main aspects. Figure 1 shows the parts of the experimental apparatus of Fermilab experiment E597 that have been used in the original analysis. The beam is coming from the left (upstream), with Cherenkov counters (C1, C2, C3) in the beam line for particle identification of the beam particles, and proportional wire chambers (A, B, C) to track the incident hadron beam trajectories. Scintillators (S1, S2, S3) provide a trigger for the associated electronics for the Downstream Particle Identifier (i.e. the part on the right of the bubble chamber). The 30-inch bubble chamber (B.C.), in a 2 T magnetic field, provides a visual target and vertex detector as well as a spectrometer for the slower produced particles. The faster particles are momentum analyzed using the fringe field of the bubble chamber magnet and a combination of proportional wire chambers (D, E) and drift chambers (F, G, H). In addition to being filled with liquid hydrogen, the bubble chamber also contains six thin foils of Mg, Ag, and Au (for each material, two foils of different thickness: for Mg, 3.7 and 11.1 *mm*; for Ag, 0.6 and 1.8 *mm*; for Au, 0.3 and 0.9 *mm*), placed in the upstream end of the chamber to provide the data on

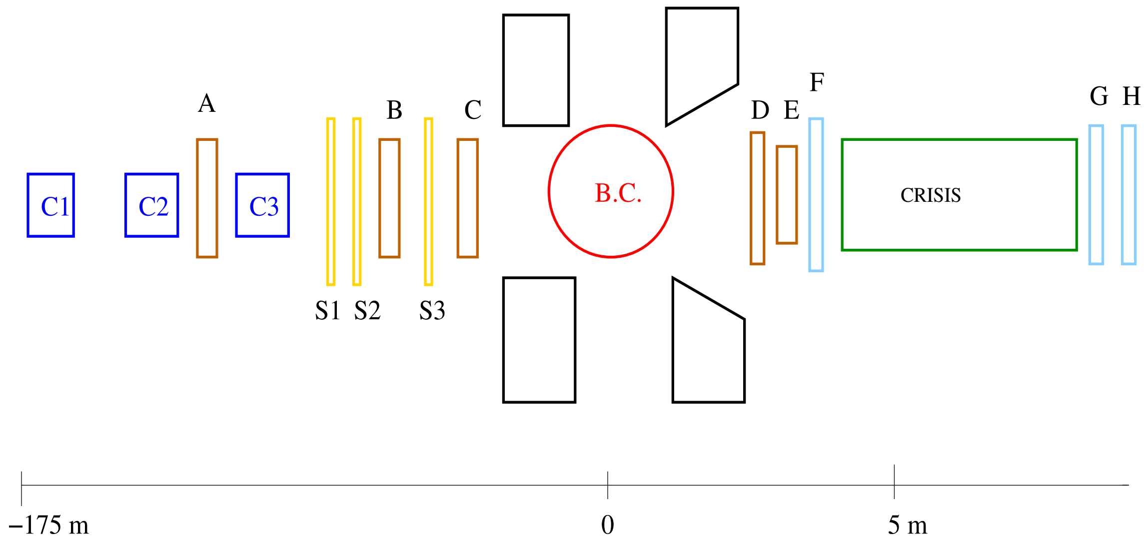

Figure 1: A schematic drawing of the parts of the experimental apparatus used in the original analysis.

hadron-nucleus interactions. CRISIS (Considerably Reduced ISIS, where ISIS (Identification of Secondaries by Ionization Sampling) was a similar but larger detector used before at CERN European Hybrid Spectrometer) is a 1 m by 1 m by 3 m ionization sampling drift chamber, which exploits the logarithmic rise in ionization for relativistic particles to provide mass identification. For particles of lower momenta, below 1.3 GeV/c, the mass identification is obtained by using the ionization loss in the bubble chamber.

The data run, in 1982, consisted of 582,000 pictures. Each bubble chamber photograph has been scanned for interactions which occurred in the thin foils of Mg, Ag, or Au. After a data selection, described in the next section, the number of hadron-nucleus events for the various combinations of beam particle and target material is reported in the Table 1.

Momentum	Beam	Mg	Ag	Au
100 GeV/c	π^-	283	773	668
	π^+	83	212	179
	K^+	21	55	60
	p	58	352	180
	$\overline{p}$	218	582	465
320 GeV/c	π^-	51	140	130

Table 1: Number of selected hadron-nucleus events.

2 Data Selection

Electromagnetic events, probably due to electrons in the beam (the beam Cherenkov counters were unable to distinguish electrons from pions) causing pair conversions in the target foils, have been classified by the following definition and then eliminated:

- charged multiplicity < 9 *and*
- $\log_{10} (< q_t^2 >) < -5$

where $< q_t^2 >$ is calculated as follows: a resultant 3-momentum vector is obtained by summing the 3-momenta of all charged particles; then the average of the square of the momentum of each charged particle in the transverse direction with respect the resultant momentum vector is evaluated.

Coherent (i.e. diffractive) events, defined as follows, have been also removed from the data sample:

- no slow protons (i.e. positive tracks with momenta < 1.3 GeV/c and identified as protons) *and*
- 3 or 5 charged tracks such that the rapidity of each of them is greater than one unit in the center-of-mass system.

We emphasize that in this analysis all fragments heavier than a proton have been labeled as "protons".
Note that elastic and quasi-elastic events do not contaminate the data sample as they were not measured (because the final states could not be distinguished from the other non-interacting beam hadrons).

3 Data distributions

The results of the analysis of inclusive single pion production

$$h + A \to \pi^{\pm} + X$$

are presented in terms of the following two distributions:

- laboratory rapidity density
$$\frac{1}{N_T}\frac{dN}{dy} \tag{1}$$
- transverse momentum squared density
$$\frac{1}{N_T}\frac{dN}{dP_t^2} \tag{2}$$

where N_T is the total number of events for a particular beam-target combination. Note that these are distribution *densities*, in the sense that they depend only on the properties of the events, but not on the number of events, so they are insensitive to the hadron-nucleus cross-sections.

The distributions reported in the paper [1] are not the ones obtained directly from the selected data sample, instead they have been corrected for the following effects, in order to facilitate the comparisons with simulations:

- misidentified $e^{\pm}$ with momenta > 200 MeV/c
  photon conversions in the target foils produce electrons and positrons; those below 200 MeV/c can be identified by ionization in the bubble chamber, whereas those above this momentum value are misidentified as pions (to correct for this contamination, a Monte Carlo method has been used, see [1] for details);

- misidentified protons
  for tracks with momenta less than 1.3 GeV/c, a correction based upon the estimated efficiency for identification of protons and pions from the ionization in the bubble chamber has been made;
  for tracks with momenta above 1.3 GeV/c, the correction of the misidentified protons is tricky, because CRISIS offers a reliable particle identification only above about 5 GeV/c: see the paper [1] for the details.

It is important to emphasize that in this experiment was not possible to separate pions from kaons, so the corrected "pion" distributions include indeed the contribution of most of charged kaons (whereas, thanks to the above corrections, we are allow to assume negligible contaminations from other non-pion particles, mainly $e^{\pm}$ and protons).

4 Fluka and Geant4 simulations

We use Geant4 [2] version 8.1.p01, with default production range threshold (0.7 mm), and with the following Physics Lists: LHEP, QGSP, and QGSC.

We use Fluka [3] version Fluka2006.3, with PRECISIO thresholds and 10 keV cut on $e^{\pm}/\gamma$, and activating the (not yet default) new high-energy model (option PEATHRES in the PHYSICS card).

As target we use a 1 μm x 1 μm x 1 mm box, with the latter dimension being the thickness seen by the beam particles (we use a single thickness for all materials only for practical convenience in running the simulation, but we did some tests with the same values as in the experiments, and we get very similar results; the motivation for such tiny transverse dimensions is to avoid of worrying about the absorption of particles produced at 90°, otherwise a correction would be needed, as done in [1]; we did also some tests with more realistic widths, without affecting the distributions).

The simulations consist simply of shooting beam particles of proper type and momentum on the target, and then printing out the information of the produced particles found at a distance of 1 cm from the target, either downstream, or upstream but going backward (i.e. in the opposite direction with respect to the beam direction), excluding $e^{\pm}/\gamma$ with momenta $<$ 200 MeV/c.

The outputs from the two simulations, Geant4 and Fluka, have the same structure, and a unique stand-alone script do the following analysis:

- remove tracks with momenta $<$ "reconstruction threshold", where as reconstruction threshold we use 100 MeV/c (the paper [1] does not specify explicitly which is the value of this threshold, but from the plots one can infer that it should be in the range 0-100 MeV/c; we have tried out different values inside this interval, with negligible changes in the physics distributions);

- remove the events that are classified as "electromagnetic", using the same definition as for the real data;

- remove the events that are classified as "coherent", using the same definition as for the real data; note that as "protons" we consider also alphas, deuterons, and tritons (we have tried out to include also some misidentified kaons as protons, or, on the other extreme, to consider pure protons without any contamination: in all these cases, no changes were observed in physics results);

- for each of the selected events, fill the distributions of laboratory rapidity and transverse momentum squared with all the charged pions and kaons in the event; note that the pion mass is used in all cases when laboratory rapidity is evaluated:
$$y = \frac{1}{2} \ln \left(\frac{E + P_L}{E - P_L} \right) \tag{3}$$
where E and P_L are the laboratory energy and longitudinal (i.e. along the beam axis) momentum, respectively.

For each combination of type of simulation (Fluka, G4 LHEP, G4 QGSP, G4 QGSC), beam particle type, beam momentum, and target material we have generated 1 million events, in such a way to have negligible statistical errors comparing with the experimental errors.

5 Results

The comparisons between Fluka simulation (red square points), Geant4 LHEP (green lower triangle points), QGSP (blue upper triangle points), QGSC (purple star points), and experimental data (black dot points) are presented in the figures 2 - 37.

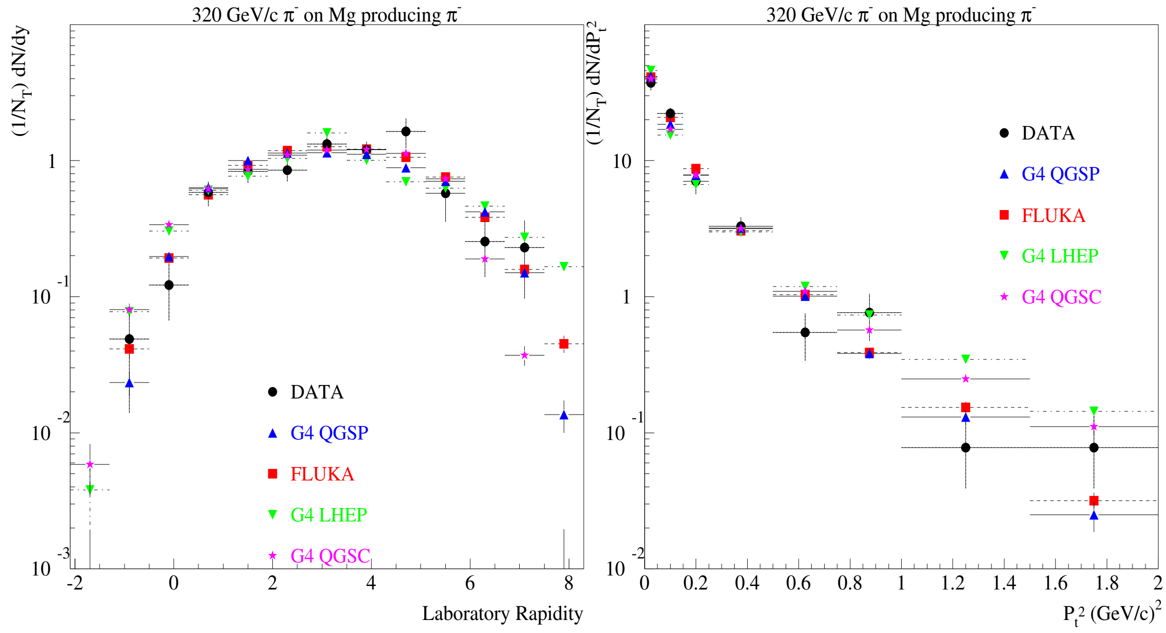

Figure 2: Laboratory rapidity (left) and transverse momentum squared (right) for π^- produced in 320 GeV/c π^- collision on Mg target.

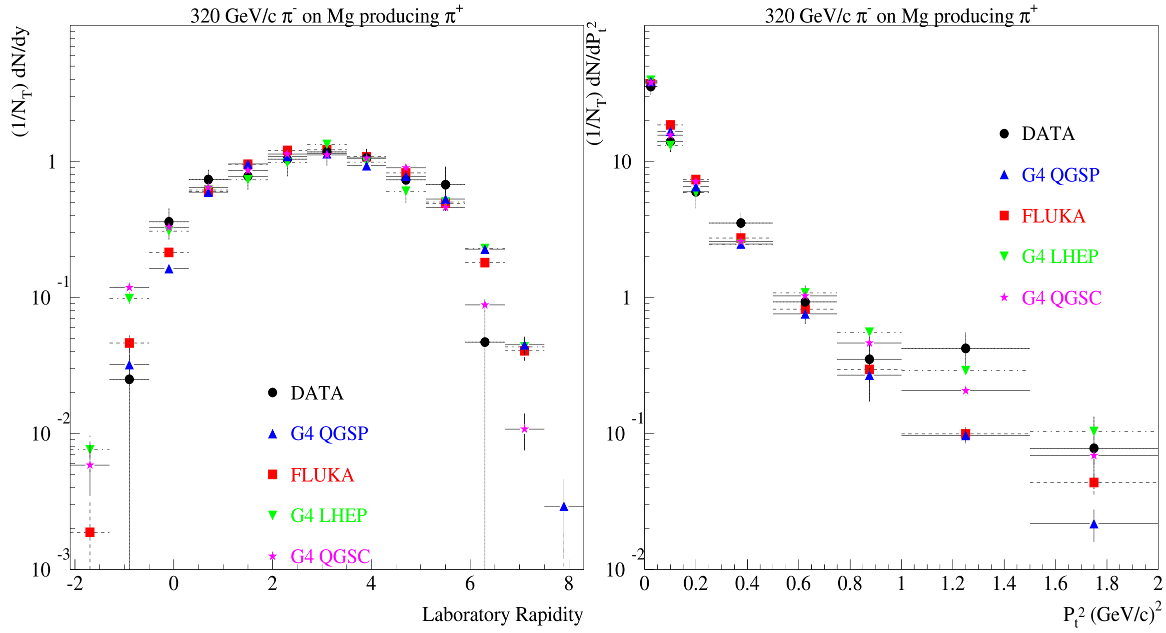

Figure 3: Laboratory rapidity (left) and transverse momentum squared (right) for π^+ produced in 320 GeV/c π^- collision on Mg target.

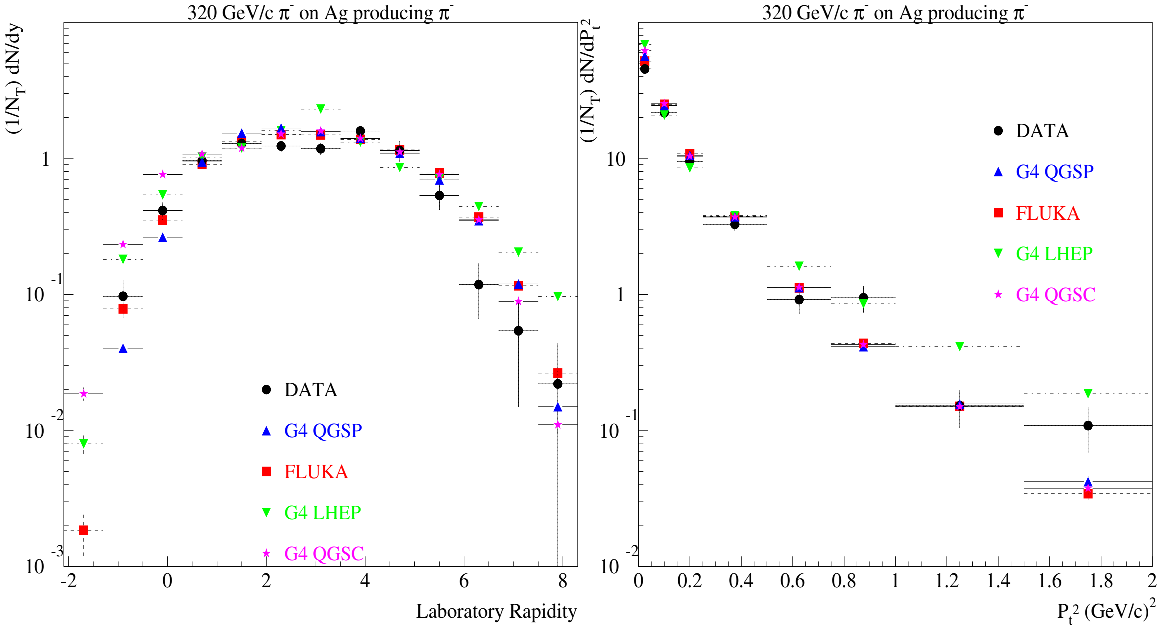

Figure 4: Laboratory rapidity (left) and transverse momentum squared (right) for π^- produced in 320 GeV/c π^- collision on Ag target.

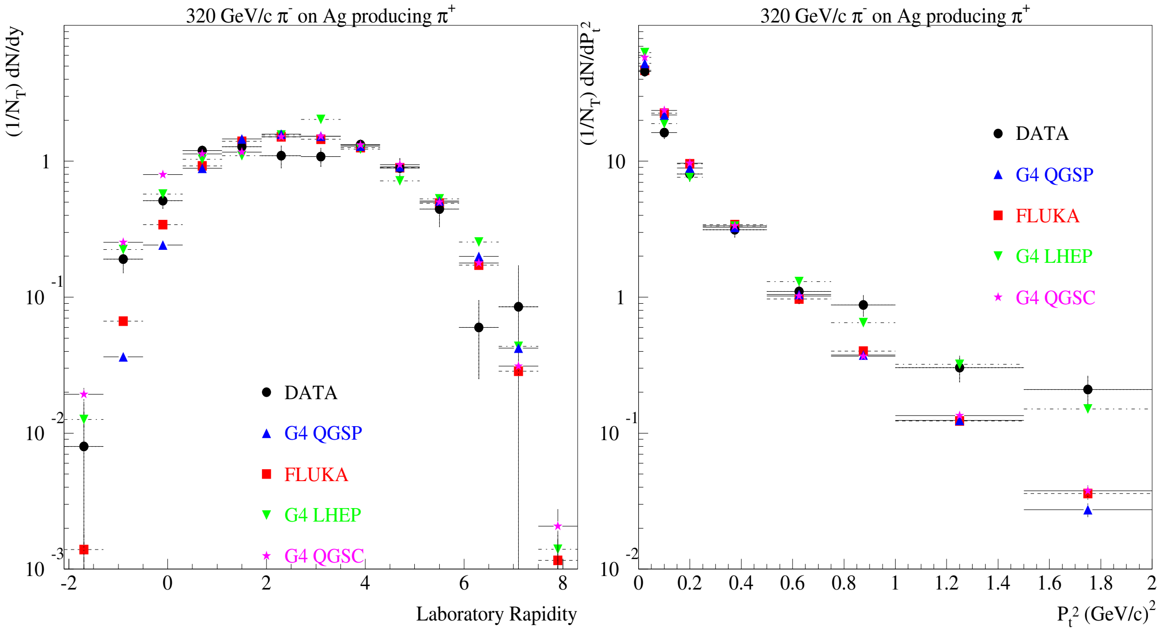

Figure 5: Laboratory rapidity (left) and transverse momentum squared (right) for π^+ produced in 320 GeV/c π^- collision on Ag target.

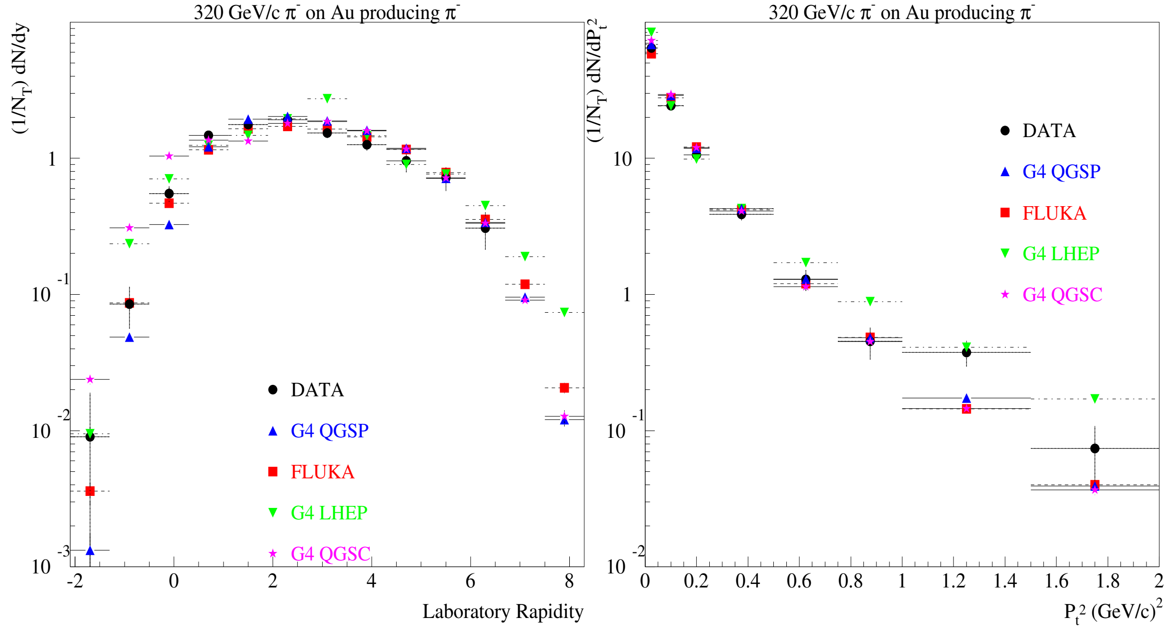

Figure 6: Laboratory rapidity (left) and transverse momentum squared (right) for π^- produced in 320 GeV/c π^- collision on Au target.

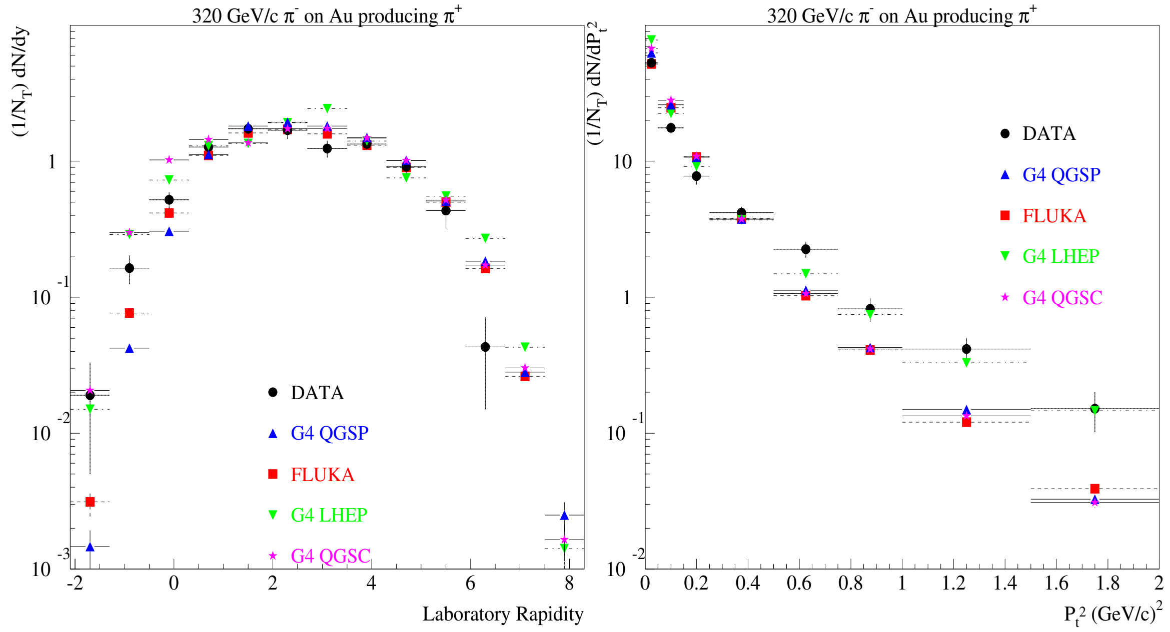

Figure 7: Laboratory rapidity (left) and transverse momentum squared (right) for π^+ produced in 320 GeV/c π^- collision on Au target.

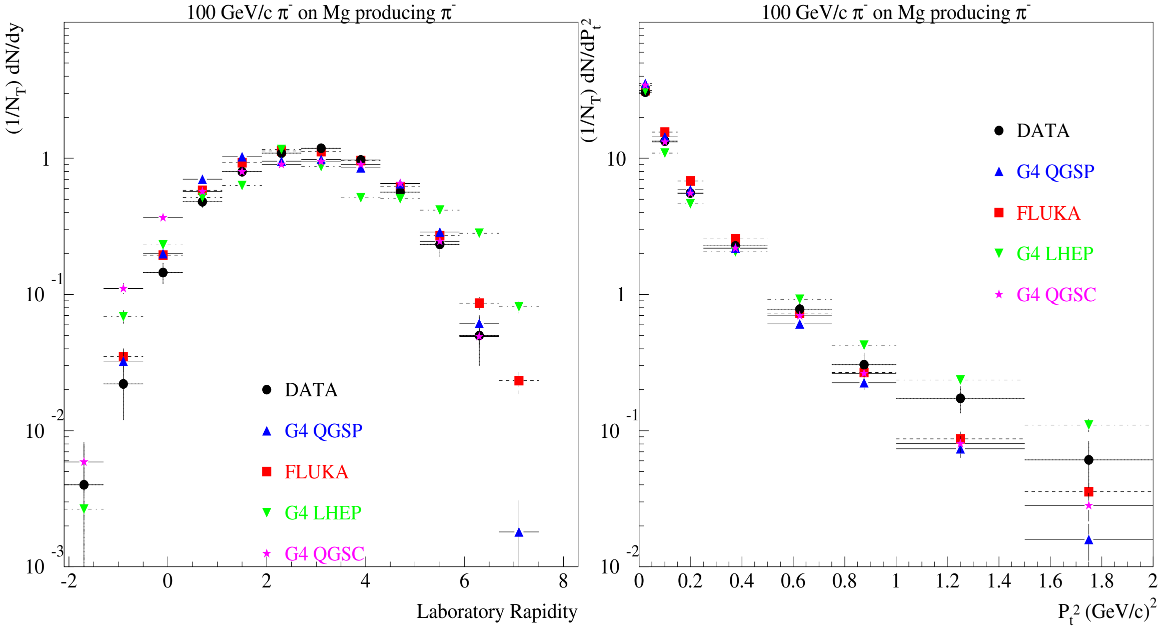

Figure 8: Laboratory rapidity (left) and transverse momentum squared (right) for π^- produced in 100 GeV/c π^- collision on Mg target.

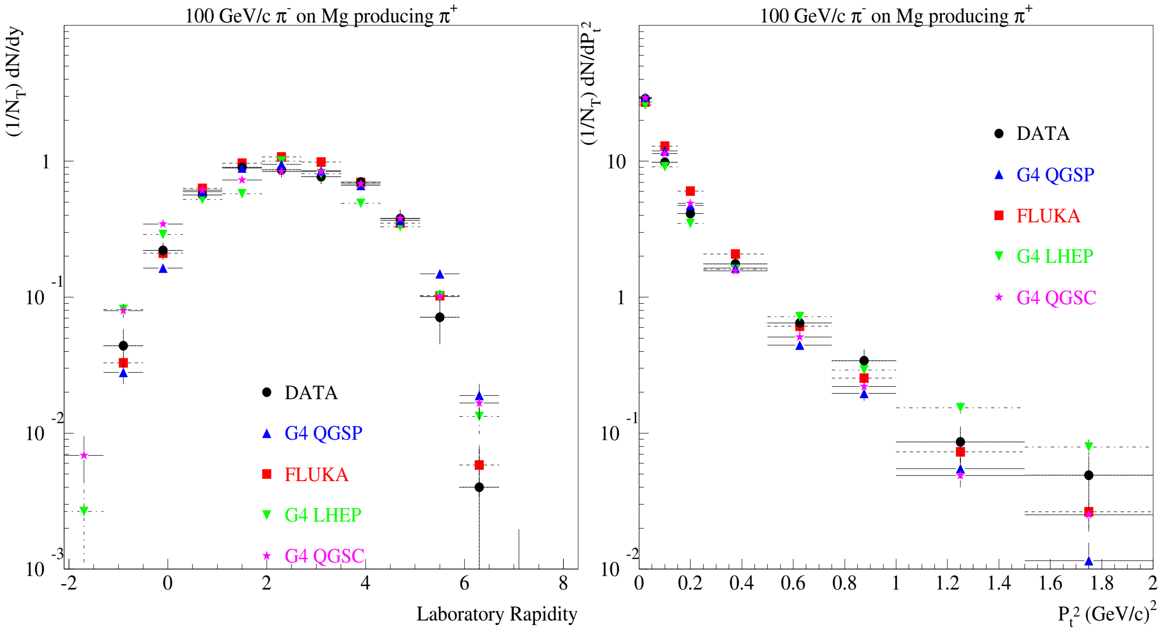

Figure 9: Laboratory rapidity (left) and transverse momentum squared (right) for π^+ produced in 100 GeV/c π^- collision on Mg target.

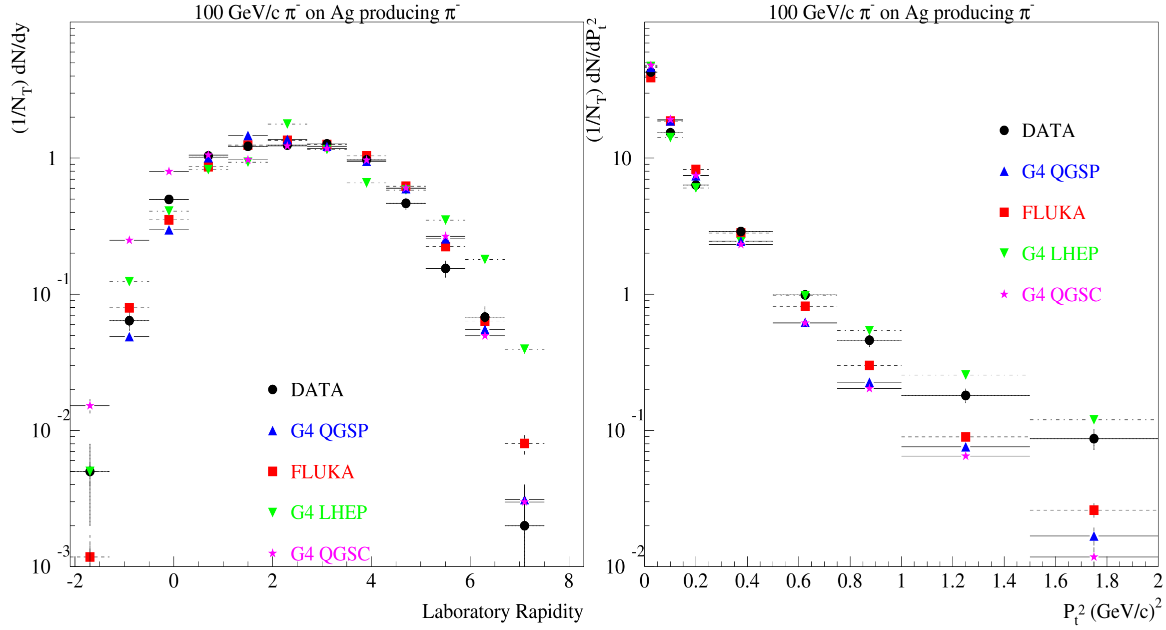

Figure 10: Laboratory rapidity (left) and transverse momentum squared (right) for π^- produced in 100 GeV/c π^- collision on Ag target.

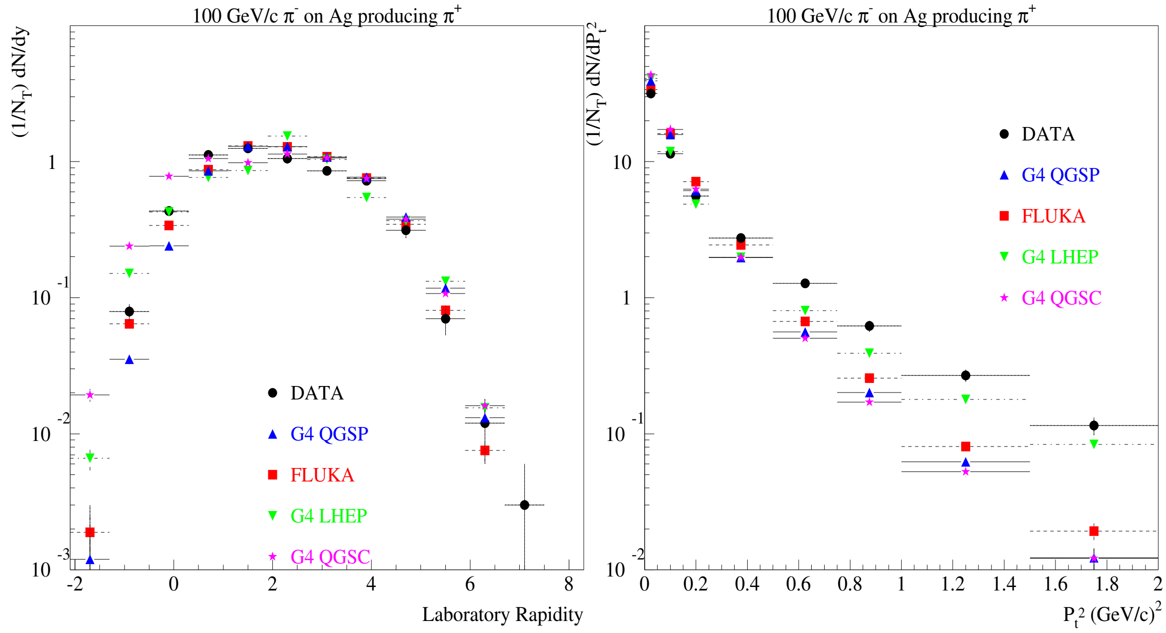

Figure 11: Laboratory rapidity (left) and transverse momentum squared (right) for π^+ produced in 100 GeV/c π^- collision on Ag target.

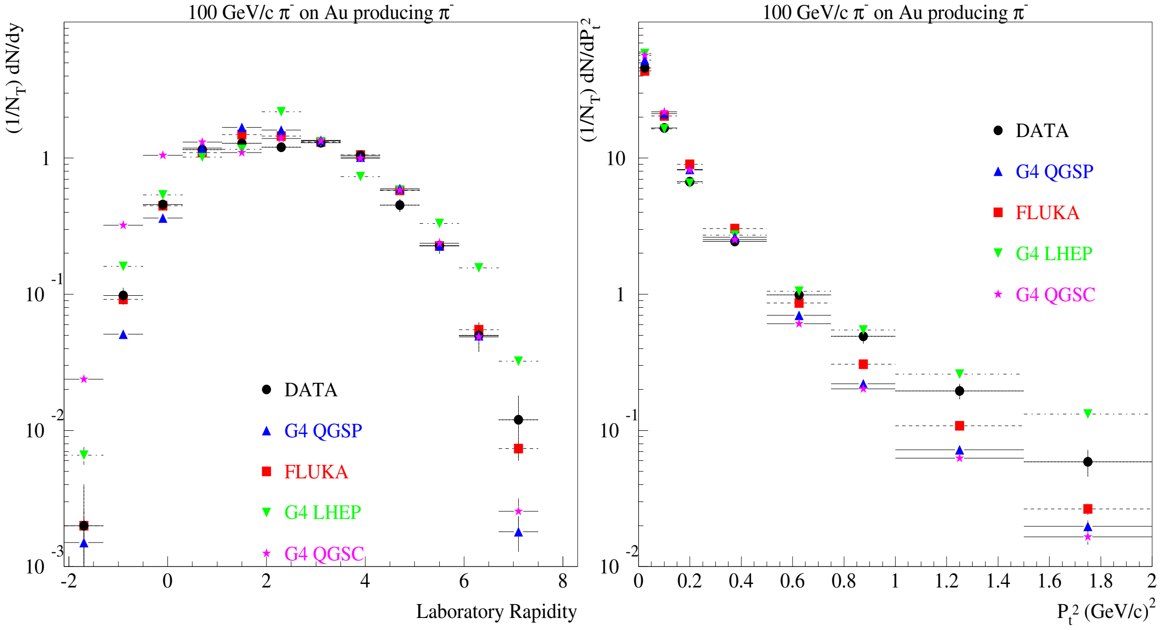

Figure 12: Laboratory rapidity (left) and transverse momentum squared (right) for π^- produced in 100 GeV/c π^- collision on Au target.

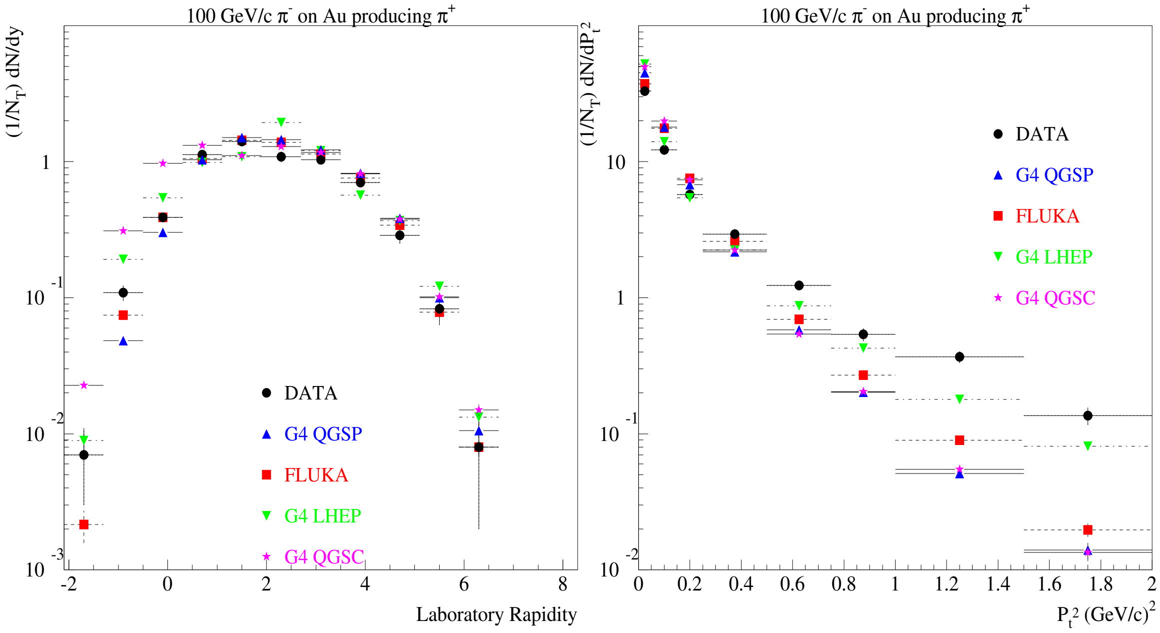

Figure 13: Laboratory rapidity (left) and transverse momentum squared (right) for π^+ produced in 100 GeV/c π^- collision on Au target.

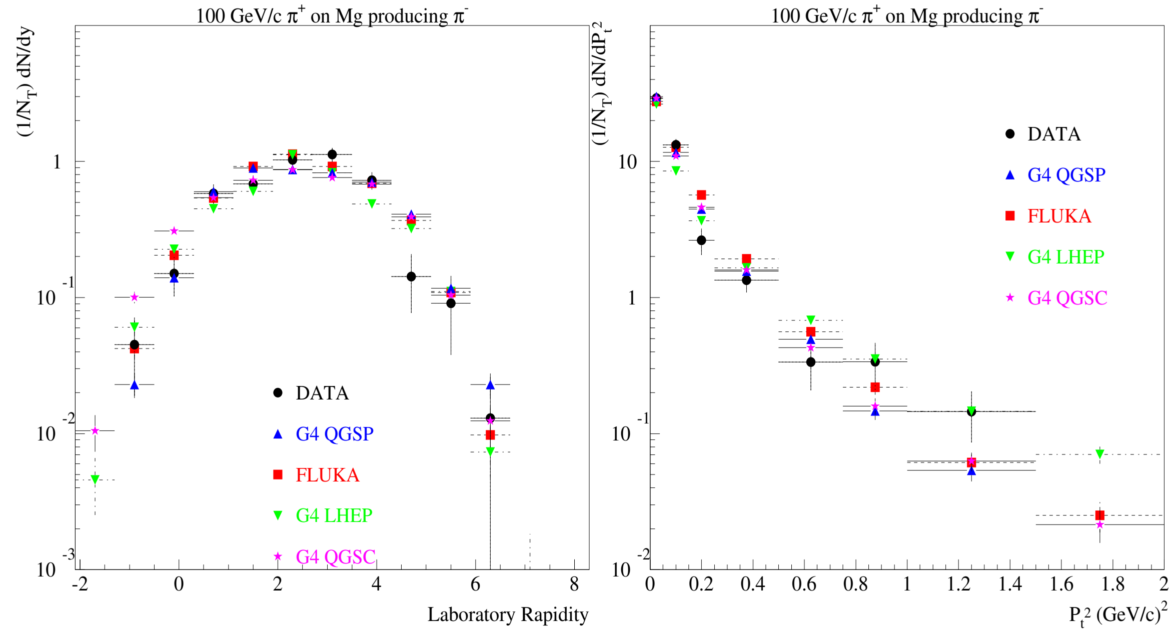

Figure 14: Laboratory rapidity (left) and transverse momentum squared (right) for π^- produced in 100 GeV/c π^+ collision on Mg target.

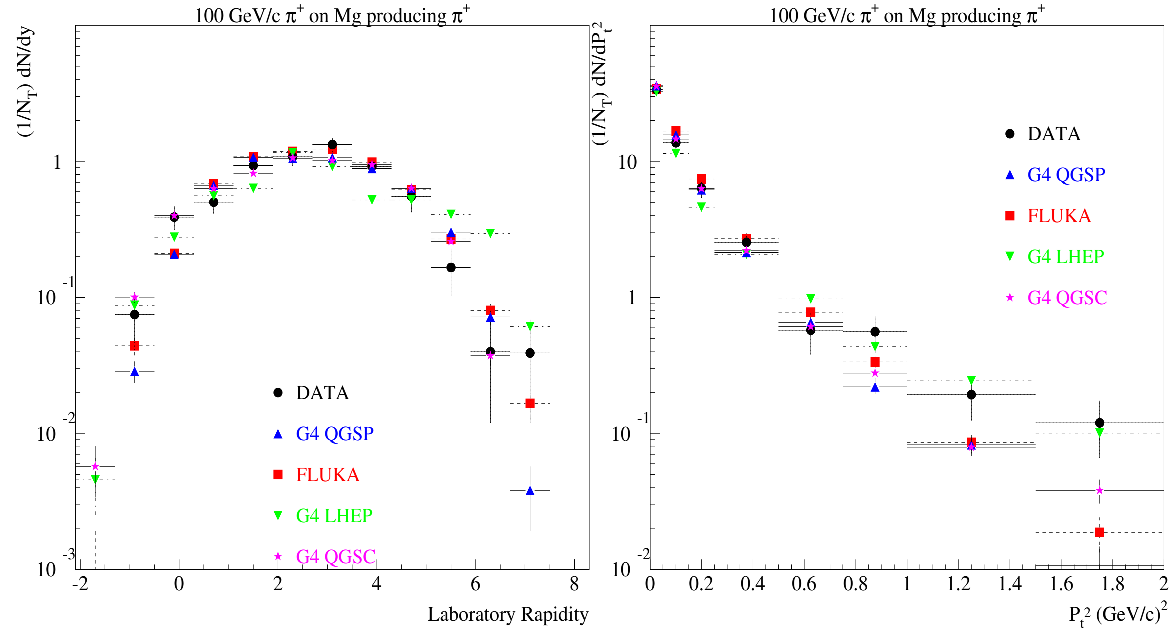

Figure 15: Laboratory rapidity (left) and transverse momentum squared (right) for π^+ produced in 100 GeV/c π^+ collision on Mg target.

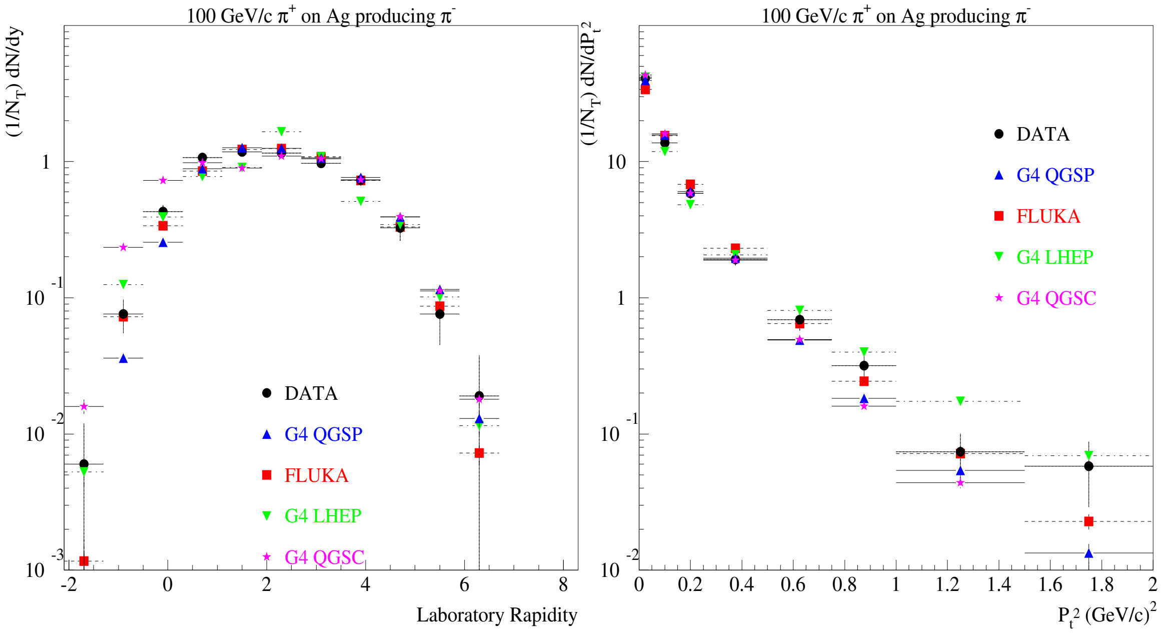

Figure 16: Laboratory rapidity (left) and transverse momentum squared (right) for π^- produced in 100 GeV/c π^+ collision on Ag target.

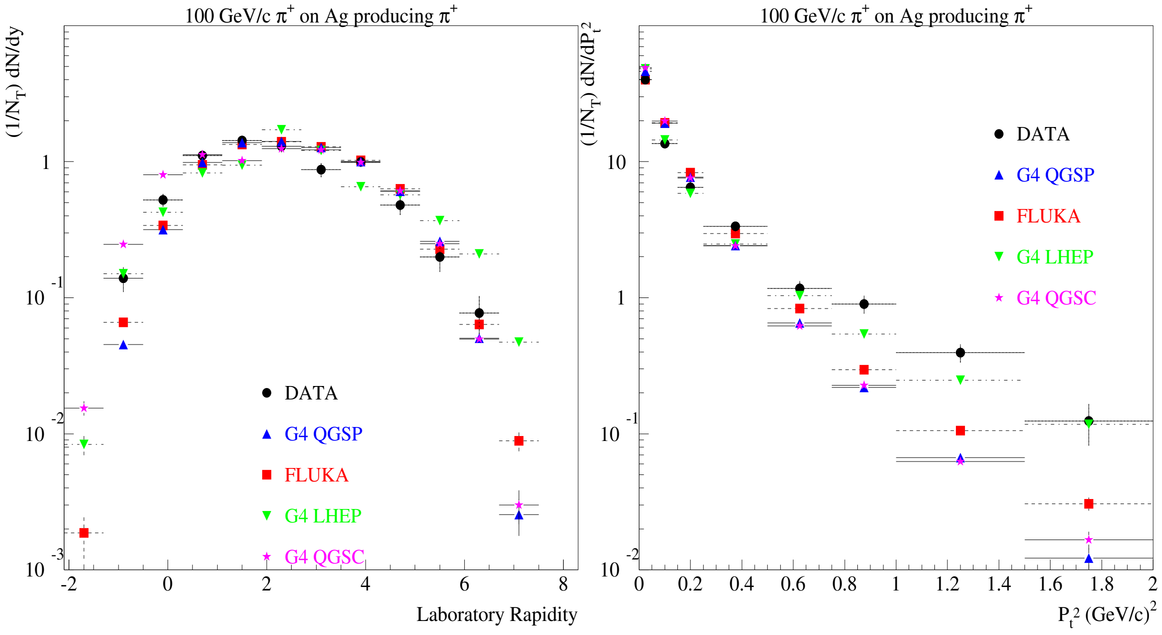

Figure 17: Laboratory rapidity (left) and transverse momentum squared (right) for π^+ produced in 100 GeV/c π^+ collision on Ag target.

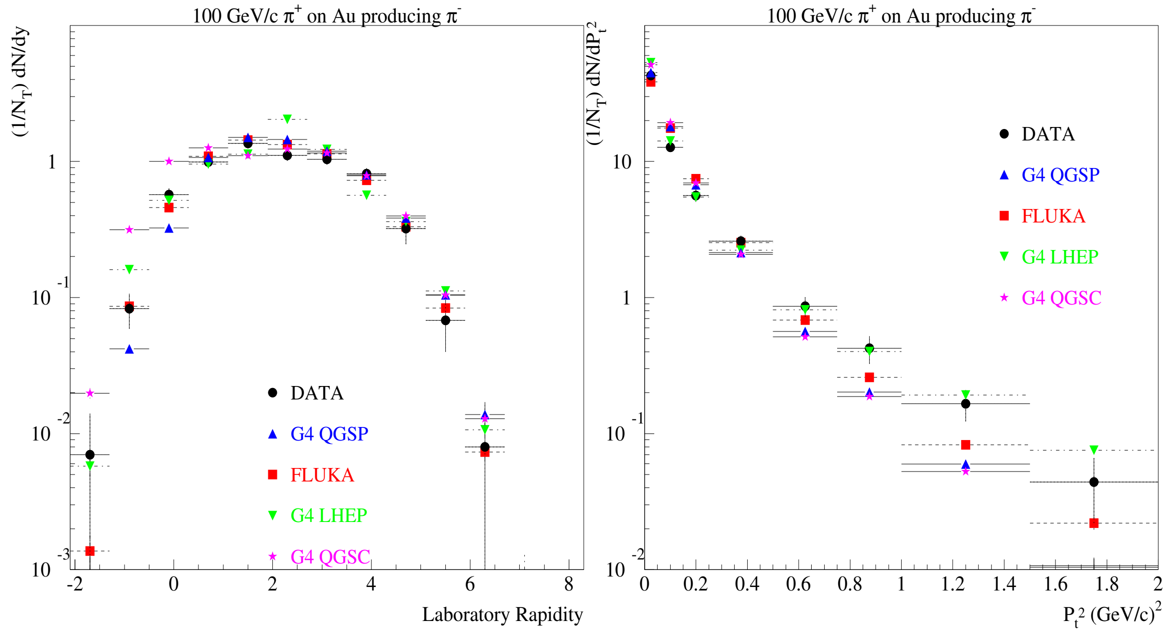

Figure 18: Laboratory rapidity (left) and transverse momentum squared (right) for π^- produced in 100 GeV/c π^+ collision on Au target.

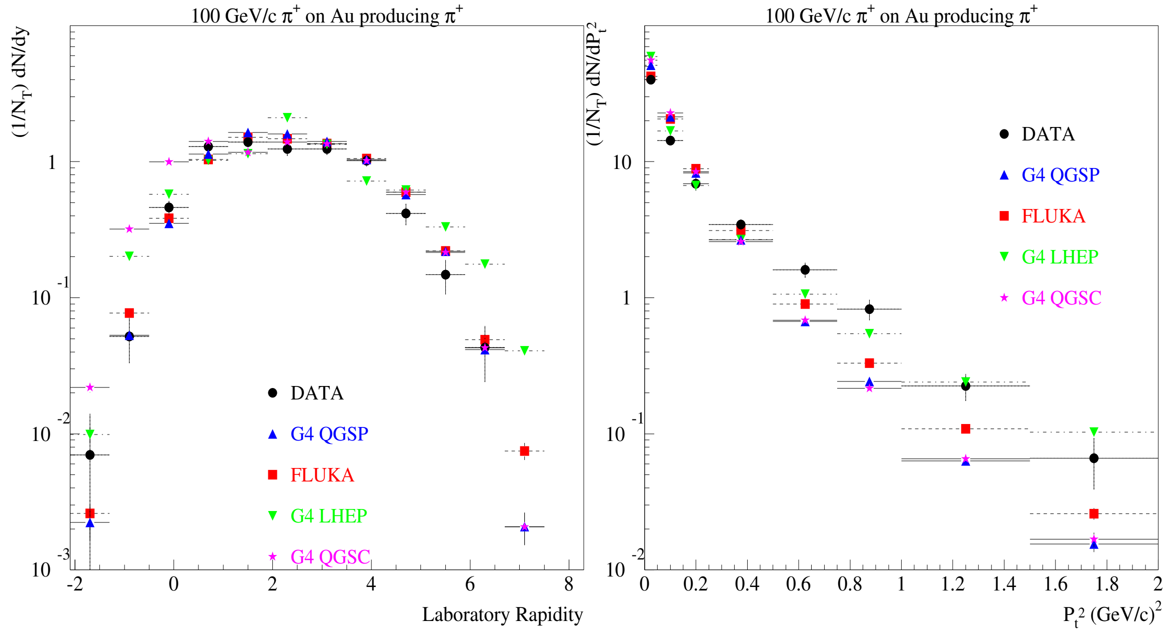

Figure 19: Laboratory rapidity (left) and transverse momentum squared (right) for π^+ produced in 100 GeV/c π^+ collision on Au target.

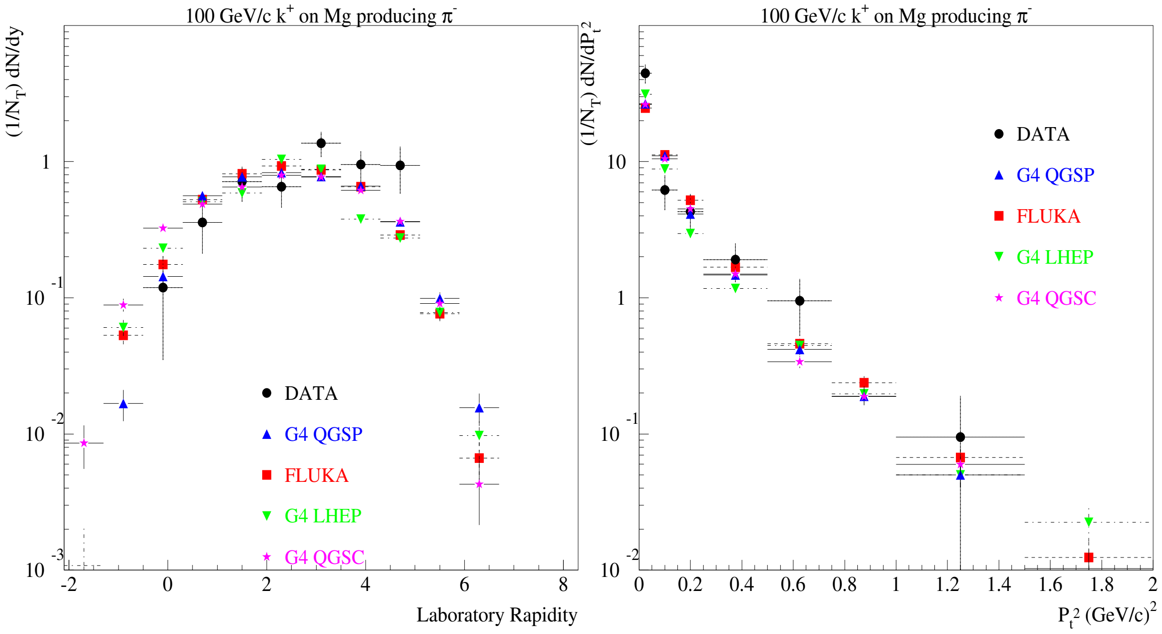

Figure 20: Laboratory rapidity (left) and transverse momentum squared (right) for π^- produced in 100 GeV/c K^+ collision on Mg target.

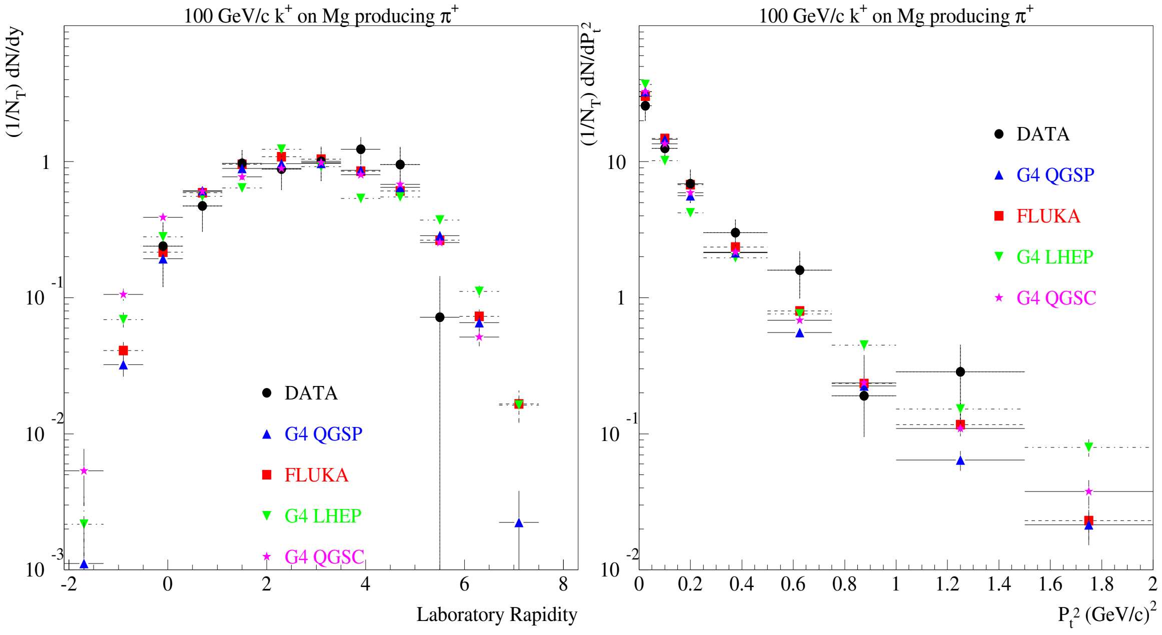

Figure 21: Laboratory rapidity (left) and transverse momentum squared (right) for π^+ produced in 100 GeV/c K^+ collision on Mg target.

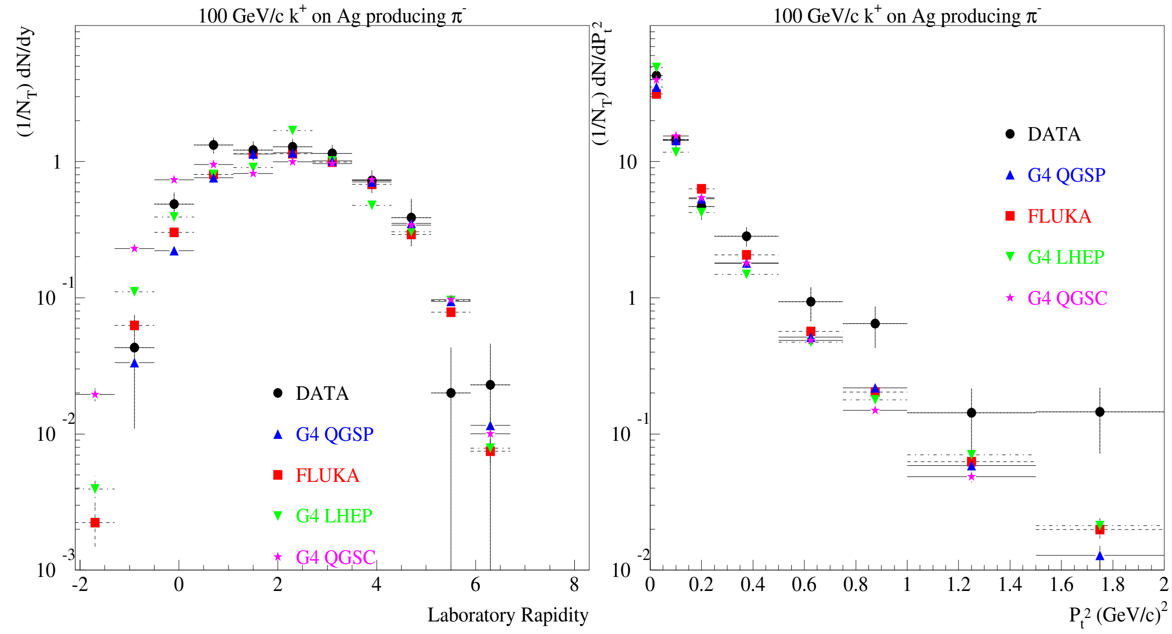

Figure 22: Laboratory rapidity (left) and transverse momentum squared (right) for π^- produced in 100 GeV/c K^+ collision on Ag target.

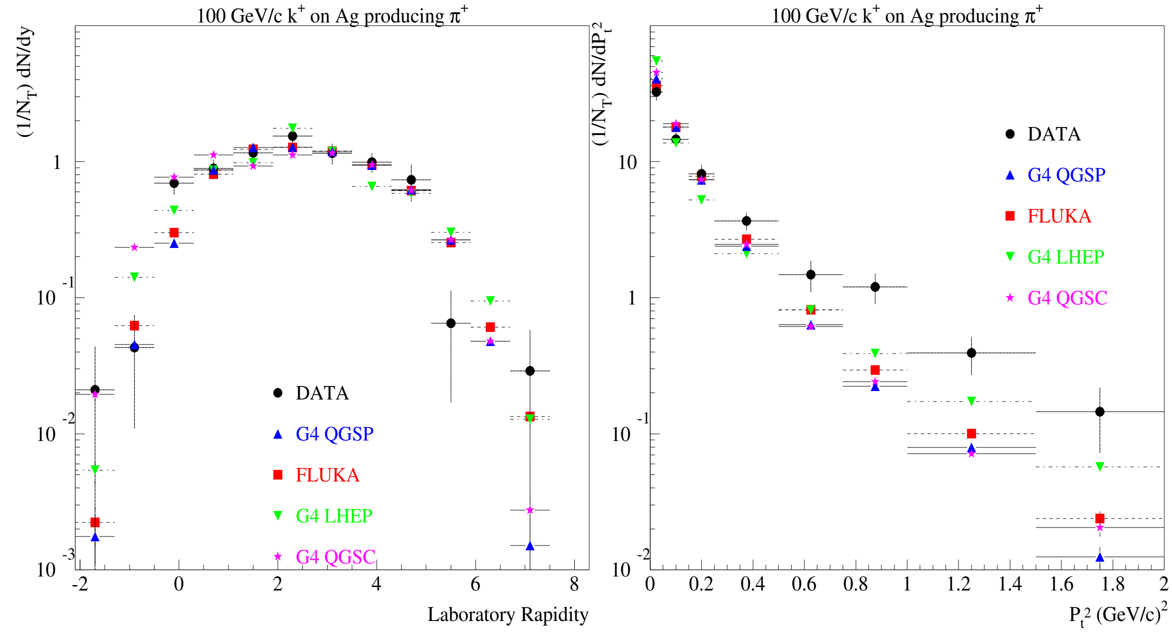

Figure 23: Laboratory rapidity (left) and transverse momentum squared (right) for π^+ produced in 100 GeV/c K^+ collision on Ag target.

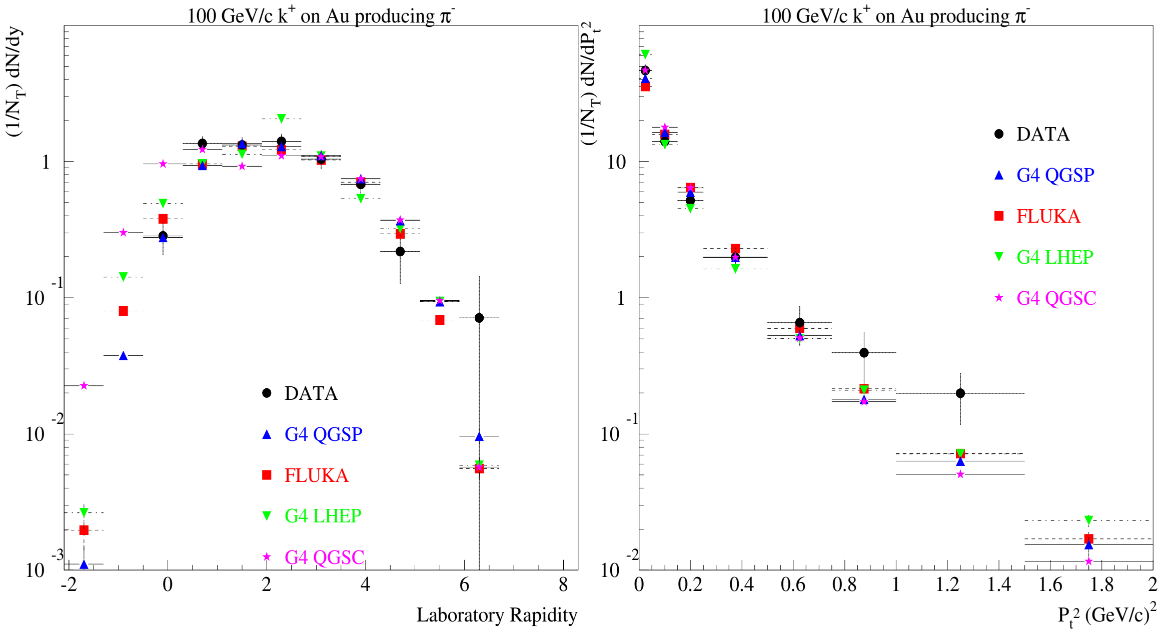

Figure 24: Laboratory rapidity (left) and transverse momentum squared (right) for π^- produced in 100 GeV/c K^+ collision on Au target.

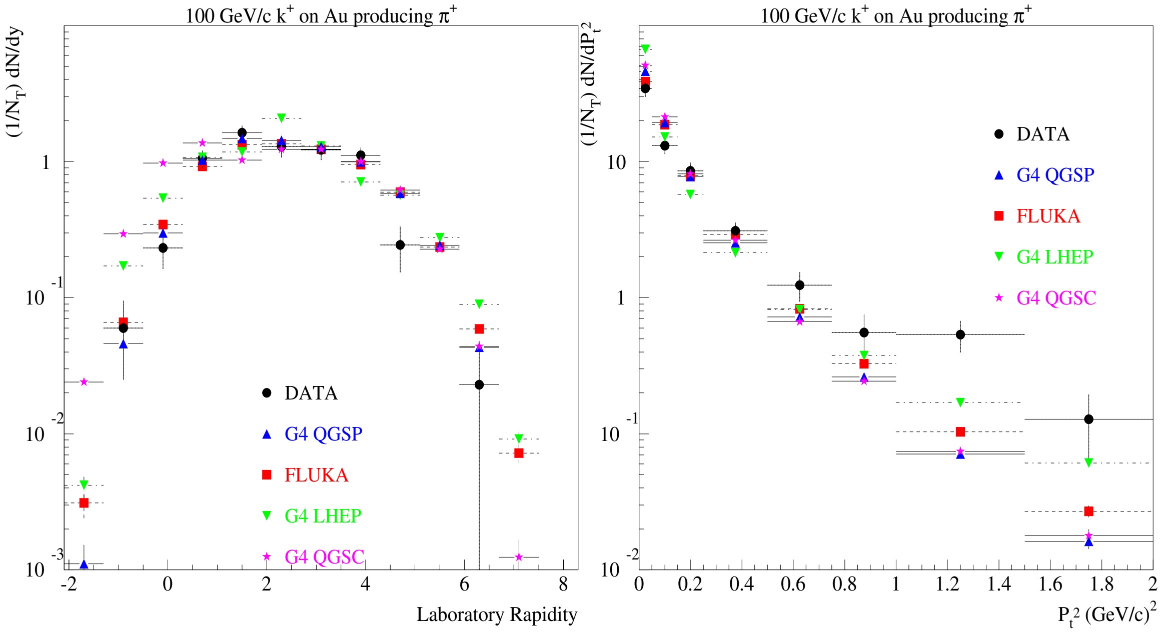

Figure 25: Laboratory rapidity (left) and transverse momentum squared (right) for π^+ produced in 100 GeV/c K^+ collision on Au target.

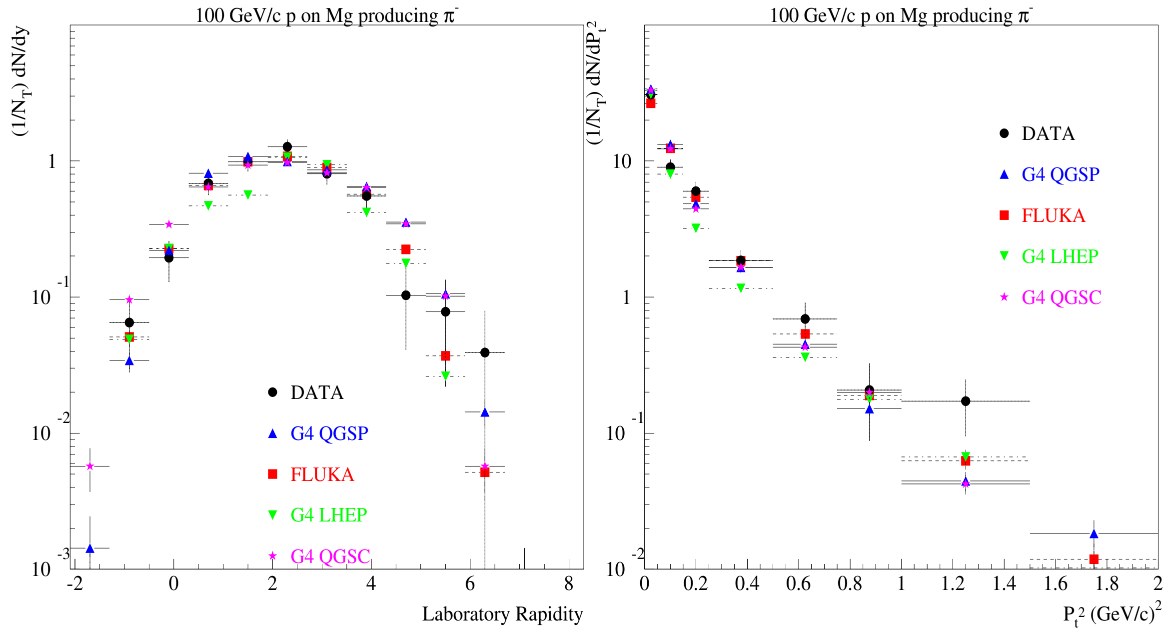

Figure 26: Laboratory rapidity (left) and transverse momentum squared (right) for π^- produced in 100 GeV/c p collision on Mg target.

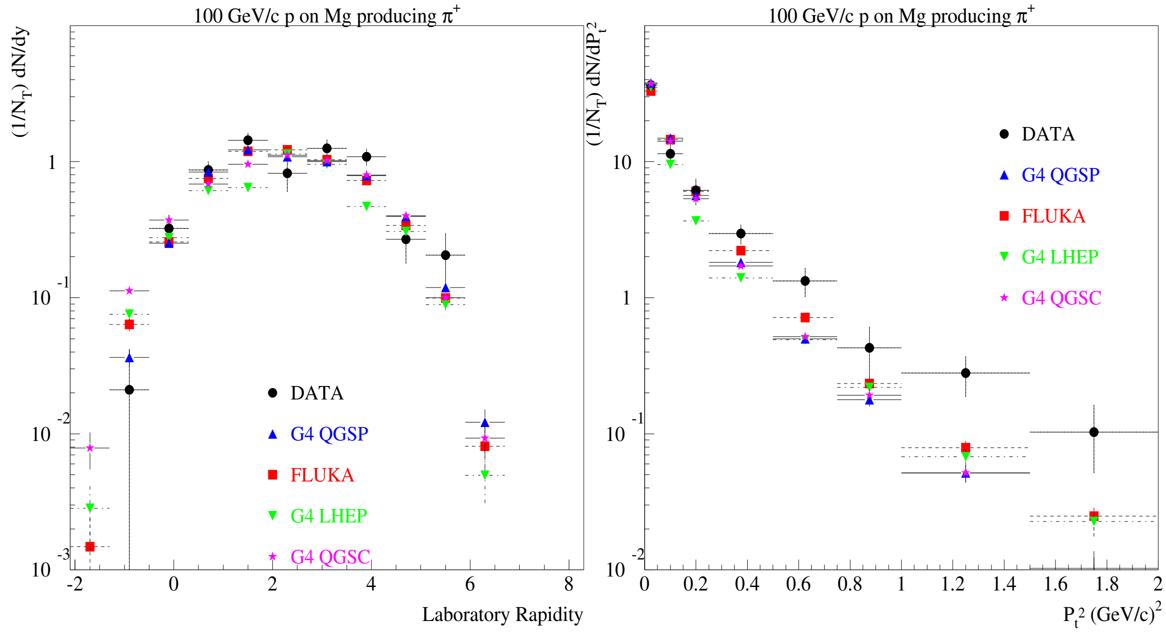

Figure 27: Laboratory rapidity (left) and transverse momentum squared (right) for π^+ produced in 100 GeV/c p collision on Mg target.

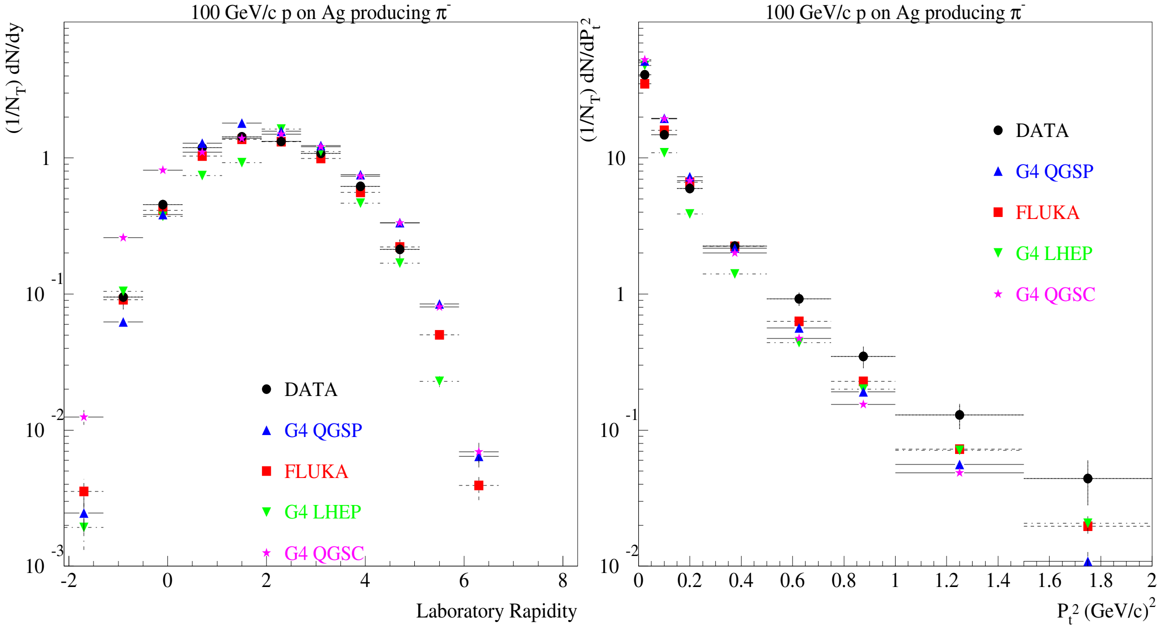

Figure 28: Laboratory rapidity (left) and transverse momentum squared (right) for π^- produced in 100 GeV/c p collision on Ag target.

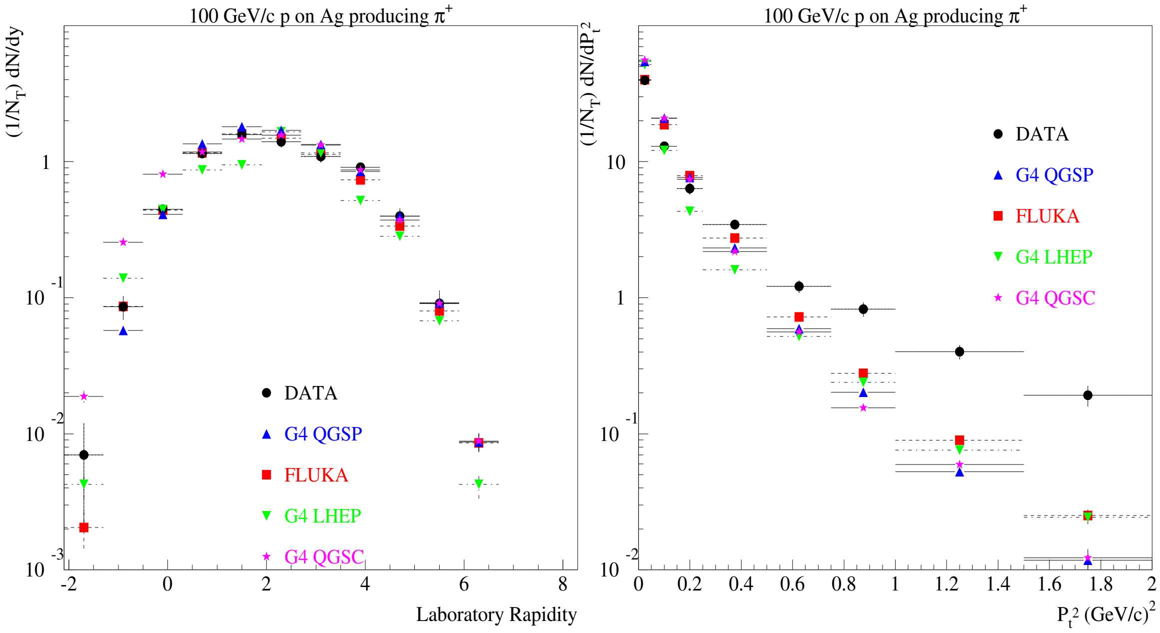

Figure 29: Laboratory rapidity (left) and transverse momentum squared (right) for π^+ produced in 100 GeV/c p collision on Ag target.

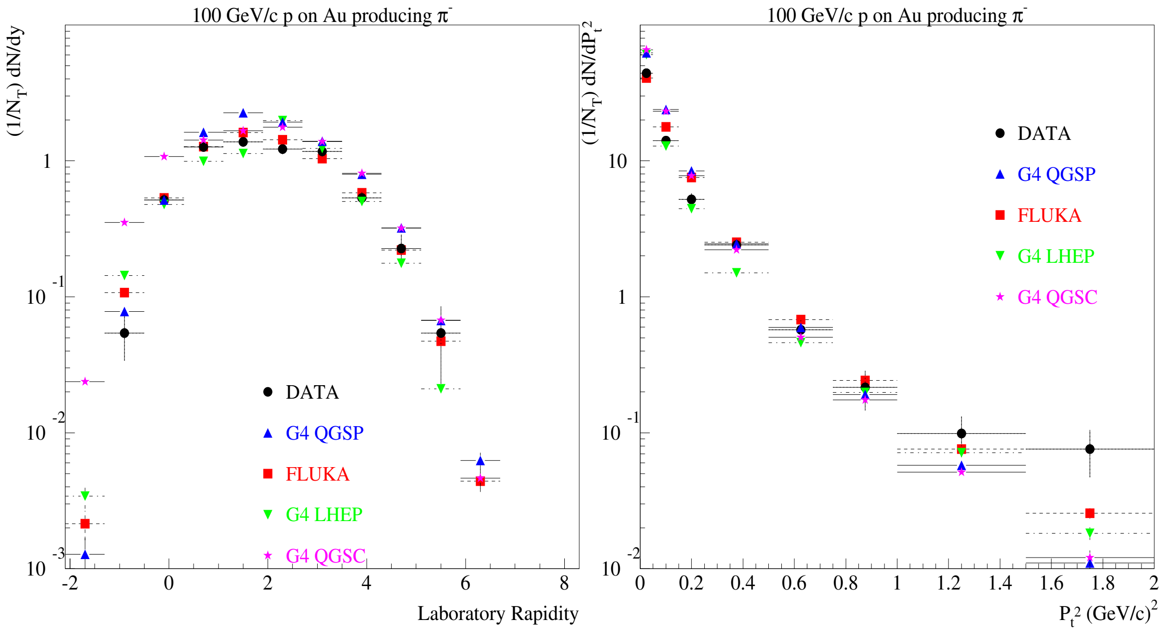

Figure 30: Laboratory rapidity (left) and transverse momentum squared (right) for π^- produced in 100 GeV/c p collision on Au target.

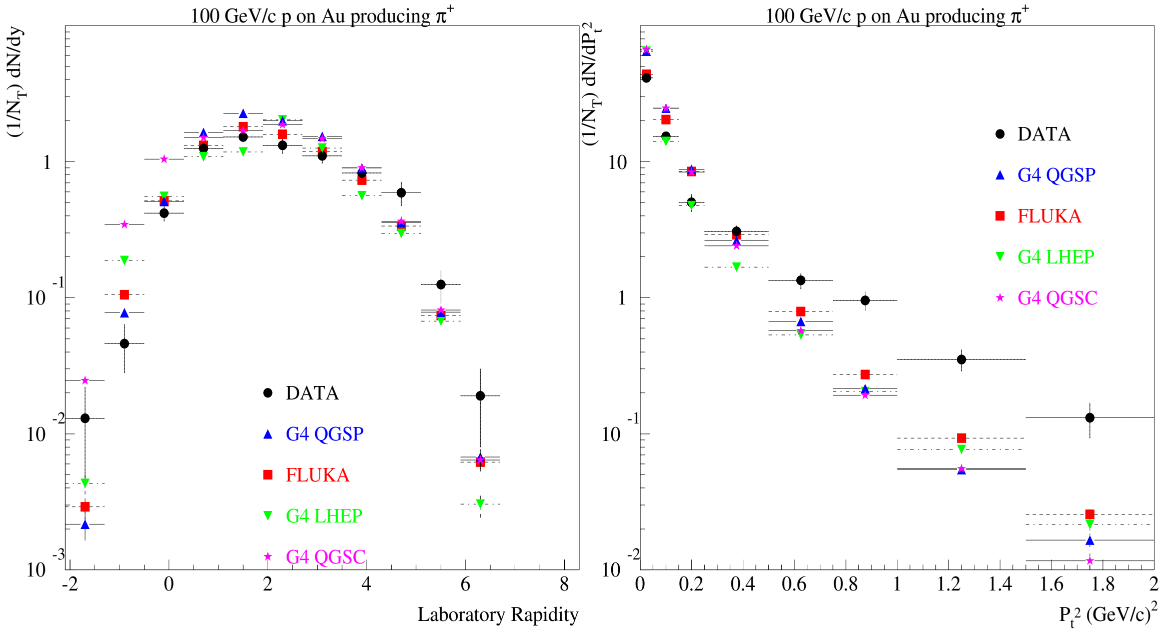

Figure 31: Laboratory rapidity (left) and transverse momentum squared (right) for π^+ produced in 100 GeV/c p collision on Au target.

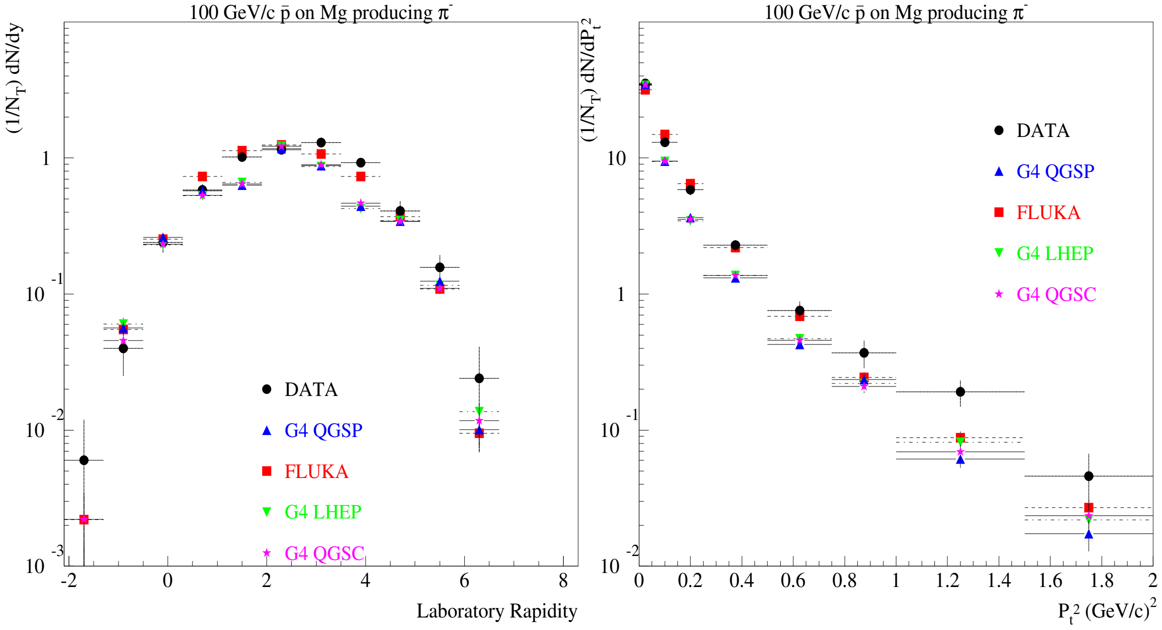

Figure 32: Laboratory rapidity (left) and transverse momentum squared (right) for π^- produced in 100 GeV/c $\overline{p}$ collision on Mg target.

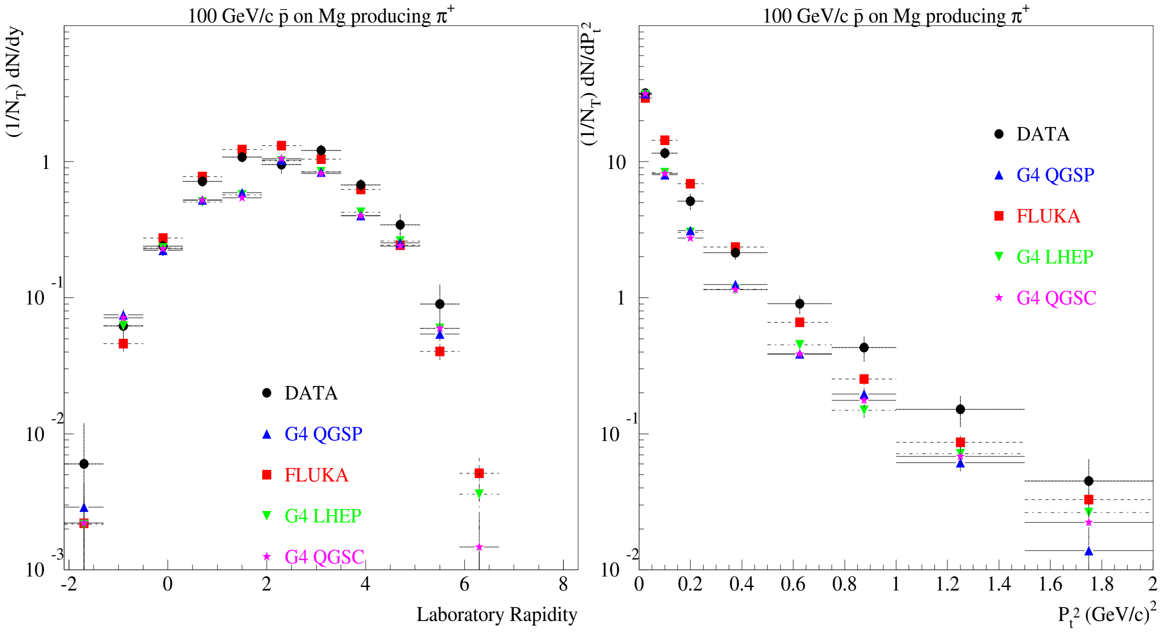

Figure 33: Laboratory rapidity (left) and transverse momentum squared (right) for π^+ produced in 100 GeV/c $\overline{p}$ collision on Mg target.

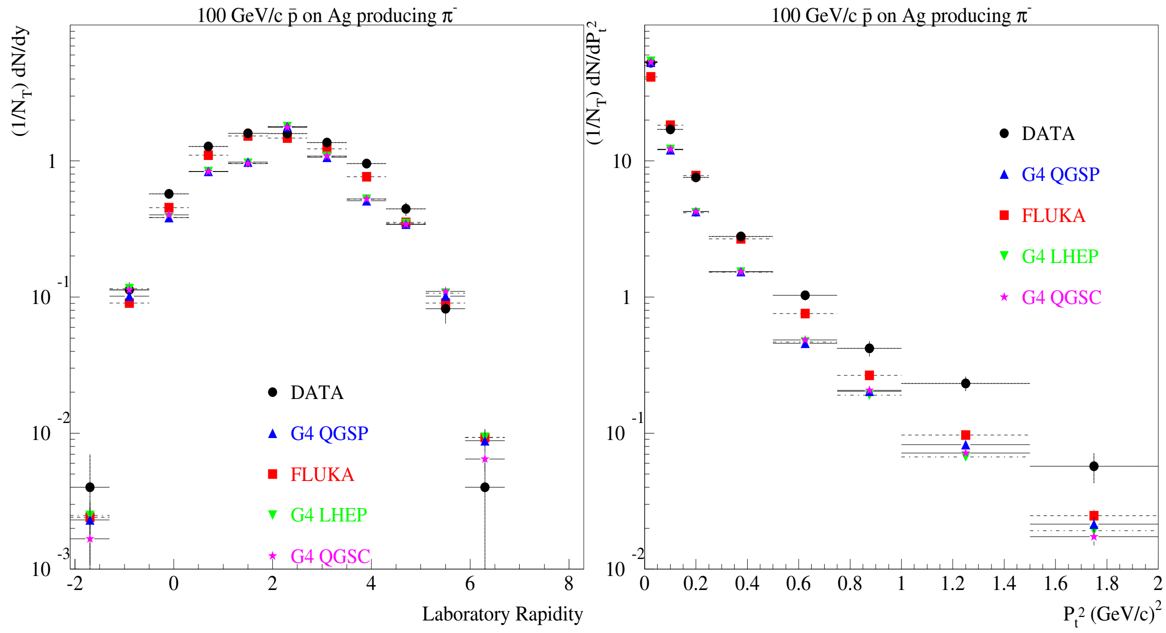

Figure 34: Laboratory rapidity (left) and transverse momentum squared (right) for π^- produced in 100 GeV/c $\overline{p}$ collision on Ag target.

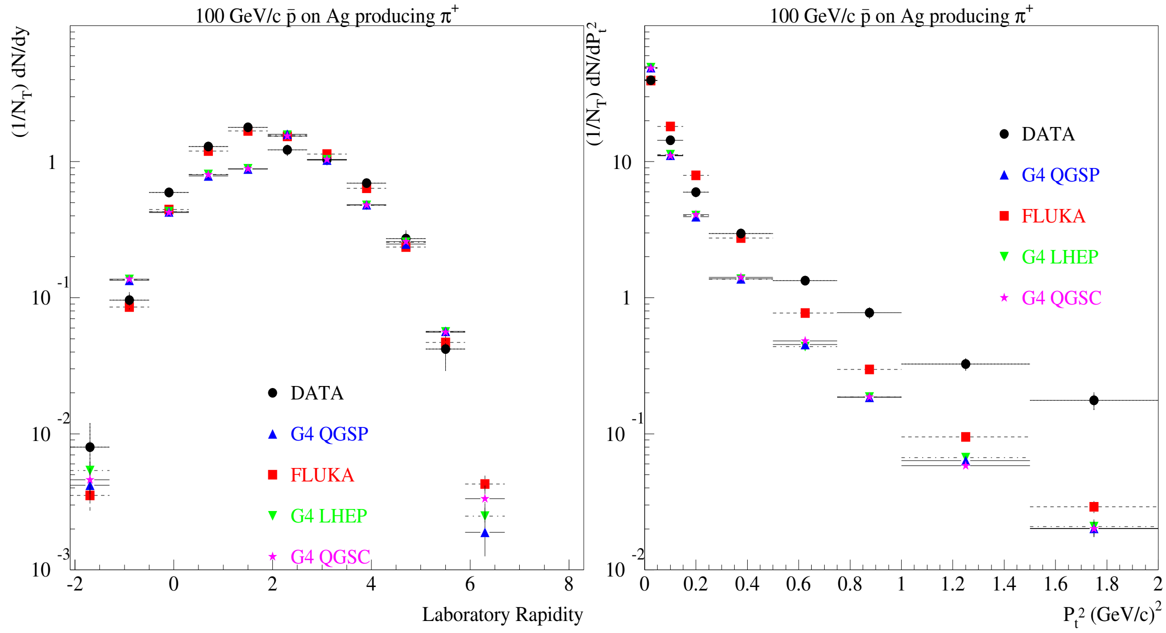

Figure 35: Laboratory rapidity (left) and transverse momentum squared (right) for π^+ produced in 100 GeV/c $\overline{p}$ collision on Ag target.

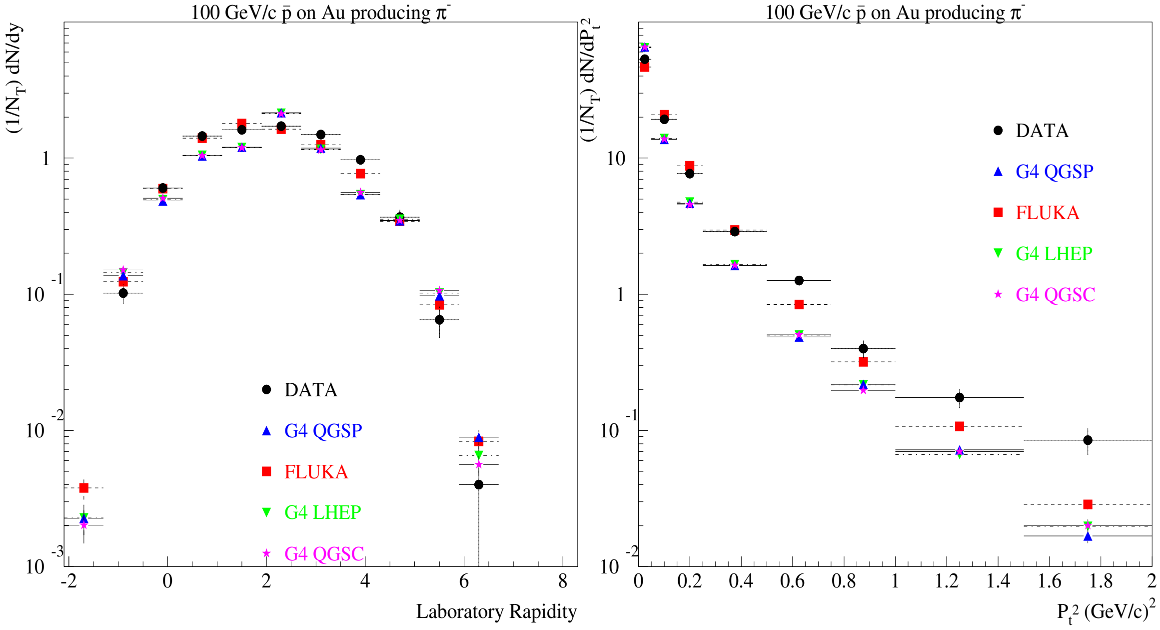

Figure 36: Laboratory rapidity (left) and transverse momentum squared (right) for π^- produced in 100 GeV/c $\overline{p}$ collision on Au target.

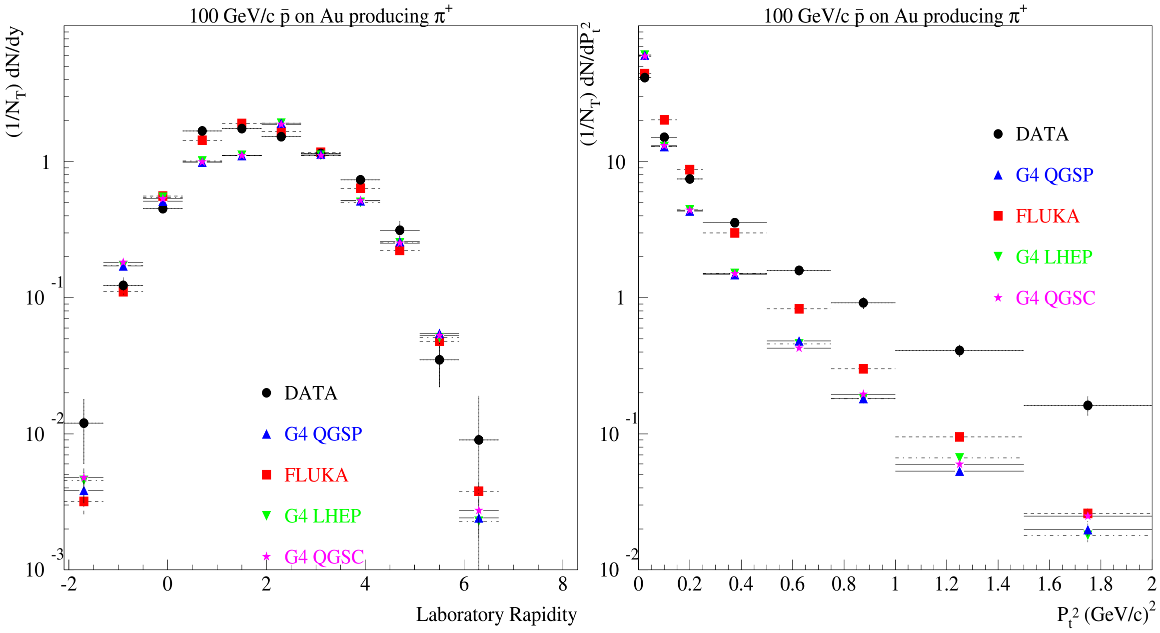

Figure 37: Laboratory rapidity (left) and transverse momentum squared (right) for π^+ produced in 100 GeV/c $\overline{p}$ collision on Au target.

6 Conclusions

In this note we have presented a thin-target benchmark of Fluka and Geant4 (LHEP, QGSP, QGSC) simulations on laboratory rapidity and transverse momentum squared of charged pions produced at 100 GeV/c and 320 GeV/c hadron-nucleus interactions, for various beam particle hadrons (π^-, π^+, K^+, p, and $\overline{p}$ at 100 GeV/c, and π^- at 320 GeV/c) and target materials (Mg, Ag, and Au), based on the data taken in a bubble chamber experiment at Fermilab.

Although the large experimental uncertainties do not allow to draw detailed quantitative conclusions, some general qualitative trends emerged. First and foremost, the results show an overall reasonable good agreement between all simulations and most of the data, with Fluka simulation showing more points of agreement. Second, for the laboratory rapidity distributions, Fluka, Geant4 QGSP and QGSC give a good description of the data; Geant4 LHEP is less accurate. Finally, for the transverse momentum squared distributions, Geant4 LHEP describes very well the data; Fluka is a bit narrower than data, while Geant4 QGSP and QGSC are narrower still.

Acknowledgment

We would like to thank John Apostolakis, Alfredo Ferrari, Gunter Folger, Mikhail Kossov, and Paola Sala for many useful discussions and suggestions.

References

[1] J.J. Whitmore et al.,
"Inclusive charged pion production in hadron-nucleus interactions at 100 and 320 GeV/c."
Z. Phys. C 62, 199-227 (1994).

[2] S. Agostinelli et al., Geant4 Collaboration,
"Geant4 - a simulation toolkit."
Nuclear Instruments and Methods in Physics Research, A 506 (2003) 250.
J. Allison et al.,
"Geant4 developments and applications."
IEEE Transactions on Nuclear Science 53 No. 1 (2006) 270-278.
See also the Geant4 web page: http://cern.ch/geant4.

[3] A. Fassò, A. Ferrari, J. Ranft, P. Sala,
"FLUKA: a multi-particle transport code."
CERN-2005-10 (2005), INFN/TC_05/11, SLAC-R-773.
A. Fassò, et al.,
"The physics models of FLUKA: status and recent developments."

Computing in High Energy and Nuclear Physics 2003 Conference (CHEP2003), La Jolla, CA, USA, March 24-28, 2003, (paper MOMT005), eConf C0303241 (2003), arXiv:hep-ph/0306267.
See also: Fluka web page: http://www.fluka.org.